Dynamic reconstruction of a numerical 2D cylinder wake flow using Data Assimilation

Nishant Kumar, Franck Kerhervé, Laurent Cordier

Dynamic reconstruction of numerical 2D-cylinder wake flow using data assimilation

N. Kumar*, F. Kerhervé, L. Cordier

Institut Pprime, CNRS – Université de Poitiers – ISAE-ENSMA, UPR 3346
11 Boulevard Marie et Pierre Curie, F86962 Futuroscope Chasseneuil Cedex, France
*Corresponding author: nishant.kumar@cnrs.pprime.fr

Abstract. The design of model-based flow controllers requires the knowledge of a dynamical model which can accurately predict the flow state. Real-time and robust estimation of the flow state however remains a challenging task when only limited spatial and temporal discrete measurements are available. In this paper, the objective is to draw upon the methodologies implemented classically in meteorology to develop dynamic observers for flow control applications. A well established data assimilation method based on Kalman filter is considered. This approach is here extended to both estimate model states and specific flow parameters. The strategy is numerically demonstrated on a POD Reduced-Order Model of a 2D-cylinder wake flow at low Reynolds number.

Keywords: data assimilation, dual ensemble Kalman filter, POD Reduced-Order Model, 2D-cylinder wake flow

1 Introduction

Despite decades of intensive research in shape optimization, aerodynamic mechanisms such as separation and mixing still represent an important source of energy expenditure in transport vehicles. The manufacturers have consequently developed, over the years, a range of strategies to improve the aerodynamic performance of their vehicles. One of these strategies consists in using active devices that can be actuated on and off based on the change of the inflow conditions. To drive such actuators, command laws and more globally valid controllers are required. To design these controllers, different strategies can be employed, one of which being the *model-based* approach. The later requires the knowledge of a dynamical model of the flow that one wants to control in real-time. In practice, the identification of such a model is challenging because it is generally obtained from limited spatial and/or time discrete informations.

This problem of state estimation is well-known in the field of meteorology where data is collected at multiple locations, with spatial and temporal scales varying in orders of magnitude, to estimate the evolution of the weather [14]. Classical methodologies involve the use of data assimilation (DA) techniques where data is assimilated, when available, with a dynamical model to correct the state estimate obtained by the model, and eventually, to correct the model itself

for further, more accurate predictions. In the specific context of aerodynamic-related problems, the complexity resides essentially in the large number of degrees of freedom of the flow dynamics, in the broad range of scales to examine and in non-linearities driving the flow system. To design a physical model that can be managed in real-time applications, the Navier-Stokes equations are traditionally projected onto an appropriate reduced basis leading to a reduced-order model of the flow [11]. Proper Orthogonal Decomposition (POD, [6]) is typically used to design the orthonormal basis which captures the flow features which are believed essential, from an energetic point of view, in representing the flow dynamics. In general, this basis is then used in a Galerkin approach to derive a POD Reduced-Order Model (POD ROM) of the flow by projecting the Navier-Stokes equations onto the POD modes. Unfortunately, this dynamical system is generally not sufficiently accurate for application in flow control, and identification methods are then used to improve the prediction ability of the POD ROM [3]. An alternative is to use the ROM in conjunction with DA techniques to design dynamic observers able to predict the flow state, provided limited information of the state itself is available [8].

In this paper, a particular stochastic DA method known as Dual Ensemble Kalman Filter (Dual EnKF) is applied to a numerical dataset of a 2D-cylinder wake flow at low Reynolds number ($Re = 100$). In the DA setup considered, time-resolved measurements of streamwise velocity component sampled at specific downstream locations serve as observations for the assimilation procedure. At the end of the assimilation window, the measurements are used to test the predictability of the DA method with respect to reproducing the flow dynamics beyond the window. In § 2, an overview of snapshot POD (§ 2.1), POD-ROM (§ 2.2), residual representation (§ 2.3), and Dual EnKF (§ 2.4) is given. POD Reduced-Order model is then applied to the cylinder wake flow in § 3. The results obtained from the application of DA to predict the dynamics of the numerical flow is discussed in § 4. Finally, the concluding remarks are given in § 5.

2 Model reduction and Ensemble Kalman Filter

In this section, we present the reduced-order modelling strategy and describe the Ensemble Kalman Filtering (EnKF) method employed for the reconstruction and prediction of the flow fields.

2.1 Snapshot POD

The proper orthogonal decomposition (POD) is a reduced-order model approach which was introduced to the fluid dynamics community as a mathematical tool to extract coherent structures from turbulent flow fields [6]. It provides an objective algorithm to decompose a set of data into a minimal number of basis functions or *modes* to capture as much as possible the information contained in the data. It is a pure *data-driven* method and as such requires only the flow field data for

modal decomposition. POD extracts the modes based on optimizing the mean square of the field variable under observation [2].

Let $\boldsymbol{\chi}$ be the spatial coordinates and t represents the scalar time, we assume that the unsteady component of the vector field $\boldsymbol{u}(\boldsymbol{\chi}, t)$ can be decomposed as

$$\boldsymbol{u}(\boldsymbol{\chi}, t) - \overline{\boldsymbol{u}}(\boldsymbol{\chi}) = \sum_i a_i(t)\boldsymbol{\phi}_i(\boldsymbol{\chi}), \tag{1}$$

where $\overline{\boldsymbol{u}}$ is the temporal mean of $\boldsymbol{u}$. In (1), $\boldsymbol{\phi}_i$ and a_i represent the spatial modes and the time-dependent projection coefficients, respectively.

The POD method requires an ensemble of snapshots of any scalar (*e.g.* pressure, temperature) or vectorial (*e.g.* velocity, vorticity) fields defined at discrete spatial points $\boldsymbol{\chi}_i$ $(i = 1, \ldots, N_\chi)$ and discrete time instants t_k $(k = 1, \ldots, N_t)$. From this data set, we prepare snapshots of the flow field stacked in terms of a collection of column vectors $\boldsymbol{u}'(\boldsymbol{\chi}_i, t_k)$ where

$$\boldsymbol{u}'(\boldsymbol{\chi}_i, t_k) = \boldsymbol{u}(\boldsymbol{\chi}_i, t_k) - \overline{\boldsymbol{u}}(\boldsymbol{\chi}_i) \in \mathbb{R}^{N_s}, \quad i = 1, 2, \ldots, N_\chi, \quad k = 1, 2, \ldots, N_t \tag{2}$$

where N_s is the number of the spatial degrees of freedom of the data. For a fluid flow data, N_s is equal to the number of grid points (N_χ) times the number of components (N_c) to be considered in the data. The snapshot vector can be stacked in matrix form as

$$\boldsymbol{X} = [\boldsymbol{u}'(\boldsymbol{\chi}_i, t_1)\ \boldsymbol{u}'(\boldsymbol{\chi}_i, t_2)\ \ldots \boldsymbol{u}'(\boldsymbol{\chi}_i, t_{N_t})] \in \mathbb{R}^{N_s \times N_t}. \tag{3}$$

Next, the objective is to find the optimal basis vectors that can best represent the flow data in an average energetic sense. In other words, we seek the vectors $\boldsymbol{\phi}_i^{\text{POD}}$ in (1) that can represent $\boldsymbol{u}'(\boldsymbol{\chi}_i, t_k)$ in an optimal manner and with the least number of modes. The solution to this problem can be determined by finding the eigenvectors $\boldsymbol{\psi}_i$ and eigenvalues λ_i from

$$\boldsymbol{X}^T\boldsymbol{X}\boldsymbol{\psi}_i = \lambda_i\boldsymbol{\psi}_i, \quad \boldsymbol{\psi}_i \in \mathbb{R}^{N_t} \tag{4}$$

where $\boldsymbol{X}^T\boldsymbol{X} \in \mathbb{R}^{N_t \times N_t}$ is a temporal correlation matrix[1]. The eigenvalues λ_i are arranged in descending order such that $\lambda_1 \geq \lambda_2 \geq \ldots \geq \lambda_{N_t} \geq 0$.

In most numerical cases, spatial size of the data is very large compared to the temporal size, $N_s \gg N_t$. For this reason, the *method of snapshots* proposed by Sirovich [13] is preferred to the classical *spatial POD method* that leads to a spatial correlation matrix $\boldsymbol{X}\boldsymbol{X}^T$ of size N_s [11].

After obtaining the eigenvectors $\boldsymbol{\psi}_i$ from the smaller eigenvalue problem (4), the (spatial) POD modes are recovered as

$$\boldsymbol{\phi}_i = \frac{1}{\sqrt{\lambda_i}}\boldsymbol{X}\boldsymbol{\psi}_i \in \mathbb{R}^{N_s}, \quad i = 1, 2, \ \ldots, N_t, \tag{5}$$

[1] For simplicity, we have considered the field data to be placed on a uniform grid. In general, the cell volume needs to be included in the formulation to represent the spatial inner product. The covariance matrix should therefore be written as $\boldsymbol{X}^T\boldsymbol{W}\boldsymbol{X}$ where $\boldsymbol{W}$ holds the spatial weights.

which can be also written as

$$\boldsymbol{\Phi} = \boldsymbol{X}\boldsymbol{\Psi}\boldsymbol{\Lambda}^{-1/2}, \tag{6}$$

where $\boldsymbol{\Phi} = [\boldsymbol{\phi}_1\ \boldsymbol{\phi}_2\ \cdots\ \boldsymbol{\phi}_{N_t}] \in \mathbb{R}^{N_s \times N_t}$ and $\boldsymbol{\Psi} = [\boldsymbol{\psi}_1\ \boldsymbol{\psi}_2\ \cdots\ \boldsymbol{\psi}_{N_t}] \in \mathbb{R}^{N_t \times N_t}$. Note that these matrices are orthonormal, *i.e.* $\boldsymbol{\Phi}^T\boldsymbol{\Phi} = \boldsymbol{\Phi}\boldsymbol{\Phi}^T = \boldsymbol{I}$ and $\boldsymbol{\Psi}^T\boldsymbol{\Psi} = \boldsymbol{\Psi}\boldsymbol{\Psi}^T = \boldsymbol{I}$ (normality of $\boldsymbol{X}^T\boldsymbol{X}$). The temporal coefficients are determined accordingly as

$$a_i(t) = \langle \boldsymbol{u}'(\boldsymbol{\chi}, t), \boldsymbol{\phi}_i(\boldsymbol{\chi}) \rangle_{\Omega}, \quad i = 1, 2, \ \ldots, N_t, \tag{7}$$

where $\langle \cdot \rangle_{\Omega}$ represents the spatial inner product defined as

$$\left\langle \boldsymbol{v}^{\mathrm{I}}(\boldsymbol{\chi}, t), \boldsymbol{v}^{\mathrm{II}}(\boldsymbol{\chi}, t) \right\rangle_{\Omega} = \int_{\Omega} \boldsymbol{v}^{\mathrm{I}}(\boldsymbol{\chi}, t) \cdot \boldsymbol{v}^{\mathrm{II}}(\boldsymbol{\chi}, t)\, \mathrm{d}\boldsymbol{\chi} \tag{8}$$

for two given vector fields $\boldsymbol{v}^{\mathrm{I}}$ and $\boldsymbol{v}^{\mathrm{II}}$ defined in a spatial domain Ω.

2.2 POD Reduced-Order Model (POD ROM)

A standard Galerkin projection is then used to derive the POD ROM. The projection of the incompressible Navier-Stokes equations onto the spatial POD modes $\boldsymbol{\phi}_i$ leads, after some algebraic manipulation [3], to the following expression,

$$\begin{cases} \dot{a}_i(t) = C_i + \sum\limits_{j=1}^{N_{\mathrm{Gal}}} L_{ij} a_j(t) + \sum\limits_{j=1}^{N_{\mathrm{Gal}}} \sum\limits_{k=j}^{N_{\mathrm{Gal}}} Q_{ijk} a_j(t) a_k(t) + \mathcal{R}_i(t) \\ \\ a_i(0) = \langle \boldsymbol{u}(\boldsymbol{\chi}, 0) - \overline{\boldsymbol{u}}(\boldsymbol{\chi}), \boldsymbol{\phi}_i(\boldsymbol{\chi}) \rangle_{\Omega} \qquad i = 1, \ldots, N_{\mathrm{Gal}} \end{cases} \tag{9}$$

where N_{Gal} is the number of POD modes kept in the Galerkin projection. The residual term $\mathcal{R}_i$ reads

$$\mathcal{R}_i(t) = \sum_{j=N_{\mathrm{Gal}}+1}^{N_t} L_{ij} a_j(t) + \sum_{j=N_{\mathrm{Gal}}+1}^{N_t} \sum_{k=j}^{N_t} Q_{ijk} a_j(t) a_k(t). \tag{10}$$

The coefficients C_i, L_{ij} and Q_{ijk} are the constant, linear and quadratic coefficients of the model equation and can be expressed as functions of the spatial eigenfunctions $\boldsymbol{\phi}_i$ and the mean field $\overline{\boldsymbol{u}}$ [3]. When the residual term $\mathcal{R}_i$ is neglected, the model reduces to a so-called reduced-order model (ROM). In practice, an energetic criterion can be used to determine the value of N_{Gal} necessary to capture the essential flow dynamics. The *relative information content* (RIC) [1] is defined as

$$\mathrm{RIC}(N_{\mathrm{Gal}}) = \sum_{i=1}^{N_{\mathrm{Gal}}} \lambda_i \Bigg/ \sum_{i=1}^{N_t} \lambda_i \ . \tag{11}$$

2.3 Representation of the residual

Due to the truncation in (9), the ROM is in general not sufficiently accurate to estimate correctly the long-term dynamics (see also the discussion in § 3.2). This truncation is equivalent to keep only the most energetic modes that are associated to the largest flow motions. As a consequence, the contribution of the viscous dissipation terms are neglected and the solution of (9) may diverge in time. To account for this truncation error, a subscale turbulence representation can be used to model the residual term $\mathcal{R}_i$. Rempfer and Fasel [10] suggested to include this dissipative effect in a linear term as a "model eddy viscosity" *i.e.*

$$\mathcal{R}_i(t) = \nu_i^T \sum_{j=1}^{N_{\text{Gal}}} L_{ij} a_j^{\text{ROM}}(t). \tag{12}$$

Finally, the POD ROM considered in this paper is thus given by,

$$\begin{cases} \dot{a}_i^{\text{ROM}}(t) \simeq C_i + \sum\limits_{j=1}^{N_{\text{Gal}}} (1+\nu_i^T) L_{ij} a_j^{\text{ROM}}(t) + \sum\limits_{j=1}^{N_{\text{Gal}}} \sum\limits_{k=j}^{N_{\text{Gal}}} Q_{ijk} a_j^{\text{ROM}}(t) a_k^{\text{ROM}}(t) \\ \\ a_i^{\text{ROM}}(0) = a_i(0) \qquad i = 1, \ldots, N_{\text{Gal}} \end{cases} \tag{13}$$

where the superscript ROM is used to separately identify the temporal coefficients obtained from the POD ROM as compared to the ones which are directly obtained from snapshot POD.

The model coefficient vector $(C_1 \ldots \; L_{11} \ldots \; Q_{111} \ldots)^T$ can be calibrated thanks to a least-mean-square procedure (L2 minimization) such as detailed in Perret et al. [9] or Cordier et al. [3]. In the current paper, the model coefficient vector is calculated once and for all, and the estimation of the model eddy viscosity ν_i^T $(i = 1, \ldots, N_{\text{Gal}})$ is done by DA.

2.4 Dual Ensemble Kalman Filter (Dual EnKF)

As the POD ROM is not sufficient in general to replicate the correct dynamics, we rely on data assimilation methods to correctly identify the model parameters. *Data assimilation* is a generic methodology which combines heterogeneous observations with the underlying dynamical principles governing the system under consideration to estimate at best the states and/or physical quantities parametrising the dynamics. Starting from a background solution and incoming imperfect information, an optimal estimation of the unknowns of the system is determined which takes into account the respective statistical confidences of the different observations.

We consider a non-linear, time-discrete dynamical system given as

$$\boldsymbol{x}_{k+1}^t = \mathcal{M}_{k,k+1}(\boldsymbol{x}_k^t, \boldsymbol{\theta}_k) + \boldsymbol{\eta}_k, \tag{14}$$

where the superscript t stands for *true*. Here, $k = 0, \ldots, N-1$ is the time index with N being the total number of time steps. The propagation of the true state

$\boldsymbol{x}_k^t \in \mathbb{R}^{N_s}$ (where N_s is the dimension of the state after spatial discretisation) from time t_k to t_{k+1} is performed by a non-linear function $\mathcal{M}_{k,k+1}$ which also depends on the model parameters vector $\boldsymbol{\theta}_k$ at time t_k. The model error $\boldsymbol{\eta}_k \sim \mathcal{N}(\mathbf{0}, \boldsymbol{Q}_k)$ is considered to be Gaussian distributed with zero mean and covariance matrix $\boldsymbol{Q}_k$. The model is initialised with an initial background state $\boldsymbol{x}_0^b$ such that $\boldsymbol{x}_0^t = \boldsymbol{x}_0^b$ with the corresponding initial covariance $\boldsymbol{Q}_0$.

In conjunction with the model equation, an observation equation is used which allows the estimated state to be corrected thanks to the available measurements. The observation vector $\boldsymbol{y}_{k+1}^o \in \mathbb{R}^{N_o}$ (where N_o is the dimension of the observations) at time t_k is related to the state by the relation

$$\boldsymbol{y}_{k+1}^o = \mathcal{H}_{k+1}(\boldsymbol{x}_{k+1}^t) + \boldsymbol{\epsilon}_{k+1}, \tag{15}$$

where $\mathcal{H}_{k+1}$ denotes the observation function (which may be non-linear), and $\boldsymbol{\epsilon}_{k+1} \sim \mathcal{N}(\mathbf{0}, \boldsymbol{R}_{k+1})$ the observation noise approximated as a Gaussian distribution with zero mean and covariance $\boldsymbol{R}_{k+1}$.

If the model parameters are known to be true, a DA method is specifically used for the state estimation. On the other hand, in practice, we frequently encounter cases where the parameters are unknown or imprecise.

One of the possible approaches to solve this dual estimation problem is to use an iterative method where the filtering is alternatively applied to estimate the state and the parameters in the course of each iteration. More precisely, the model parameters are obtained from the corrected state at the previous time state and the new state is evaluated from the current analysed parameters. This method, formally known as Dual EnKF [7], consists of a sequential double prediction-correction scheme at the basis of the mechanism of evolution of the traditional Kalman filter, one for the update of the parameter vector, one for the update of the state variable.

Prediction-correction of the parameters vector

First, an ensemble of N_e forecasted parameters is created using a forced random walk of the parameters set up according to a Gaussian law $\boldsymbol{\xi}_k \sim \mathcal{N}(\mathbf{0}, \boldsymbol{C}_k)$ with zero mean and covariance matrix $\boldsymbol{C}_k$. During the prediction step, the ensemble of forecasted parameters is constructed as

$$\boldsymbol{\theta}_{k+1}^{f,(n)} = \boldsymbol{\theta}_k^{a,(n)} + \boldsymbol{\xi}_k^{(n)} \quad n = 1, \ldots, N_e \tag{16}$$

where the superscript (n) represents the n-th member of the ensemble of parameters, while the superscripts f and a denote the forecasted (predicted) and assimilated (corrected) values of the parameters, respectively. The predicted ensemble of parameters are then updated using the available observations. For this, the predicted state at the instant t_{k+1} is computed as,

$$\boldsymbol{x}_{k+1}^{f,(n)} = \mathcal{M}_{k,k+1}(\boldsymbol{x}_k^{a,(n)}, \boldsymbol{\theta}_{k+1}^{f,(n)}) \quad n = 1, \ldots, N_e. \tag{17}$$

The predicted ensemble of observations is then obtained as,

$$\boldsymbol{y}_{k+1}^{f,(n)} = \mathcal{H}_{k+1}(\boldsymbol{x}_{k+1}^{f,(n)}) \quad n = 1, \ldots, N_e. \tag{18}$$

Next, the random observations are built to be centred around the actual observation $\boldsymbol{y}_{k+1}^{o}$ following

$$\boldsymbol{y}_{k+1}^{o,(n)} = \boldsymbol{y}_{k+1}^{o} + \boldsymbol{\epsilon}_{k+1}^{o,(n)} \quad n = 1, \ldots, N_e \tag{19}$$

where the covariance matrix of the observation error at the instant t_{k+1} is given as

$$\boldsymbol{R}_{k+1}^{e} = \frac{1}{N_e - 1} \sum_{n=1}^{N_e} (\boldsymbol{\epsilon}_{k+1}^{o,(n)})(\boldsymbol{\epsilon}_{k+1}^{o,(n)})^T. \tag{20}$$

Given the random observations from (19) and the empirical estimator (20), the update of the predicted ensemble of parameters is obtained by the Kalman analysis step which reads as,

$$\boldsymbol{\theta}_{k+1}^{a,(n)} = \boldsymbol{\theta}_{k+1}^{f,(n)} + \boldsymbol{K}_{k+1}^{\theta,e}(\boldsymbol{y}_{k+1}^{o,(n)} - \boldsymbol{y}_{k+1}^{f,(n)}). \tag{21}$$

The Kalman gain allowing the correction of the parameter trajectories is expressed using the ensemble predictions as

$$\boldsymbol{K}_{k+1}^{\theta,e} = \boldsymbol{P}_{\theta y,k+1}^{f,e}(\boldsymbol{P}_{yy,k+1}^{f,e} + \boldsymbol{R}_{k+1}^{e})^{-1}. \tag{22}$$

In this expression, the terms $\boldsymbol{P}_{\theta y,k+1}^{f,e}$ and $\boldsymbol{P}_{yy,k+1}^{f,e}$ designate the unbiased empirical estimators of the cross-correlation matrix between the parameters and the observations, and the correlations between the observations, respectively.

Prediction-correction of the state variable

Once the predicted parameters have been updated, the second filter is implemented to estimate the state variable at the instant t_{k+1} by assuming the parameters as known. In other words, the parameters just corrected by the first filter are trusted. The following prediction-correction mechanism is identical to the classical ensemble Kalman filter. In the first step, the predicted ensemble of states at the instant t_{k+1} is built starting from the ensemble of assimilated states at the instant t_k and the corrected ensemble of parameters at the instant t_{k+1} *i.e.*

$$\boldsymbol{x}_{k+1}^{f,(n)} = \mathcal{M}_{k,k+1}(\boldsymbol{x}_{k}^{a,(n)}, \boldsymbol{\theta}_{k+1}^{a,(n)}) + \boldsymbol{\eta}_{k}^{(n)}. \tag{23}$$

For the second time, a forecast ensemble of observations is calculated as

$$\boldsymbol{y}_{k+1}^{f,(n)} = \mathcal{H}_{k+1}(\boldsymbol{x}_{k+1}^{f,(n)}). \tag{24}$$

At this stage, the observations are again considered as random variables and the covariance matrix of the observation error involved in calculating the Kalman gain is also empirically estimated. Next, the update of the predicted ensemble of the state is realised by Kalman analysis, given as

$$\boldsymbol{x}_{k+1}^{a,(n)} = \boldsymbol{x}_{k+1}^{f,(n)} + \boldsymbol{K}_{k+1}^{e}(\boldsymbol{y}_{k+1}^{o,(n)} - \boldsymbol{y}_{k+1}^{f,(n)}). \tag{25}$$

The use of a Kalman gain permits the correction of the state trajectories as

$$\boldsymbol{K}_{k+1}^{e} = \boldsymbol{P}_{xy,k+1}^{f,e}(\boldsymbol{P}_{yy,k+1}^{f,e} + \boldsymbol{R}_{k+1}^{e})^{-1}. \tag{26}$$

In this expression, $\boldsymbol{P}_{xy,k+1}^{f,e}$ and $\boldsymbol{P}_{yy,k+1}^{f,e}$ denote the unbiased empirical estimators of the cross-correlation matrix between the state and the observations, and the correlation matrix between the observations, respectively.

This double prediction-correction scheme is sequentially repeated over time. Note that the step of prediction-correction of the system state can precede the operation on the parameters without consequence on the quality of the estimation. We can now return to the POD ROM and present the use of the Dual EnKF method to correctly identify the model parameters. In the DA problem, the temporal coefficients $a_i^{\mathrm{ROM}}(t_k)$ form the state vector $\boldsymbol{x}_k$. The POD ROM in (13) serves as the dynamical model $\mathcal{M}_{k,k+1}$ with the model eddy viscosity ν_i^T as parameters $\boldsymbol{\theta}$. The initial background condition $\boldsymbol{x}_0^b$ is same as the POD temporal coefficients. Finally, as will be discussed in § 4.1, the observations vector $\boldsymbol{y}_k^o$ is built using velocity measurements in the computational domain.

Following the so-called *representers' formulation* proposed by Evensen and Leeuwen [4], the Kalman analysis equations (25) and (26) can be used to characterise the effect of the probe location on the estimated fields. The representers give an estimate of the expected value of the cross correlation between the state and measurements. The influence vectors correspond to the columns of $\boldsymbol{P}_{xy,k+1}^{f,e}$ and the magnitudes are given by the product $(\boldsymbol{P}_{yy,k+1}^{f,e}+\boldsymbol{R}_{k+1}^{e})^{-1}(\boldsymbol{y}_{k+1}^{o,(n)}-\boldsymbol{y}_{k+1}^{f,(n)})$. The influence vectors give the areas in the computational domain where the corrections from the measurements take place and the magnitudes give the level of correction [see 12]. This framework will be used in §4.1 to analyse the effect of the measurements' locations.

3 Dynamical modelling of a 2D-cylinder wake flow

In order to test the data assimilation framework in a simple numerical configuration, we choose to estimate the dynamics of a 2D-cylinder wake flow. The snapshots necessary to determine the POD modes (see § 2.1) are obtained from a numerical simulation. A POD reduced-order model is then built using the procedure described in § 2.2. This POD ROM serves as the dynamical model used for the application of the Dual EnKF method described in § 2.4.

3.1 Numerical simulation

The numerical simulations are performed using a finite-element based incompressible Navier-Stokes equations solver in *FreeFem++* [5]. The computational domain along with the dimensions and boundary conditions is shown in Fig. 1. All the dimensions have been parametrised with the diameter of the cylinder D, here set to one. For the purpose of mesh size control, the domain is divided into

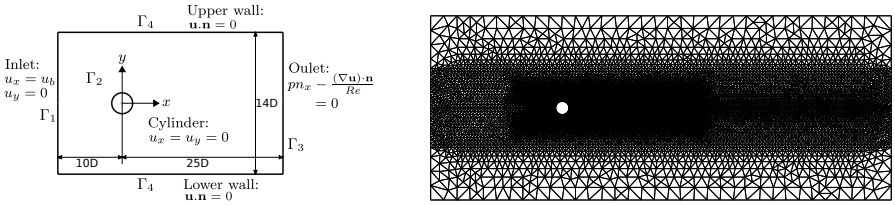

(a) (b)

Fig. 1: (a) Schematic of the computational domain and boundary conditions for the 2D-cylinder wake flow. (b) Finite-element discretisation of the domain obtained from *FreeFem++*.

sub-domains and the automatic mesh generation offered by the `buildmesh` command in *FreeFem++* is used. The mesh has 10263 vertices and 20360 triangles.

To solve the space discretised Navier-Stokes equations, an optimised Newton method is used. This approach is a variant of the classical Newton method for which the non-linear term is discretised semi-implicitly. The velocity and pressure variables are discretised using $P2$ and $P1$ finite element spaces, respectively. After convergence of the iterative procedure, the pressure field is such that the resulting velocity is divergence free.

The Reynolds number of the numerical simulation based on the cylinder diameter D is set to $Re = 100$. The snapshots are taken in a time range of $[150, 250]$ s after all initial disturbances have been damped. The simulation generates $N_t = 1000$ snapshots at a sampling frequency of $f_s = 10$ Hz. The snapshots contain the information of the two components of the fluctuating velocity vector $\boldsymbol{u}' = [u'_x, u'_y]^T$. The number of degrees of freedom for the problem (size of the discretised state variables) is $N_s = 81772$. The time evolution of the drag and lift coefficient are shown in Fig. 2. From the evolution, it is observed that after the initial transient phase, the periodic vortex shedding is observed from $t = 100$ s onwards. This implies that the snapshots will represent the dynamics of the post-transient stable vortex shedding over the whole assimilation window.

3.2 Characterisation of POD ROM

The POD modes are calculated for the fluctuating velocity fields obtained from the snapshot database. The energy content of the modes is plotted in Fig. 3. We observe that the first ten modes together represent 99.98% of the energy. Therefore, for the further evaluation of the ROM, we reduce the number of modes to $N_{\text{Gal}} = 10$, where $N_{\text{Gal}} \ll N_t$.

The most dominant temporal and spatial modes are plotted in Fig. 4 and Fig. 5, respectively. From now on, the coefficients and modes obtained by POD will be denoted with the superscript POD. The amplitude of the temporal coefficients a_i^{POD} for the first pair (a_1^{POD}, a_2^{POD}) is greater by an order of magnitude when compared with the next pair of modes (a_3^{POD}, a_4^{POD}). For the following

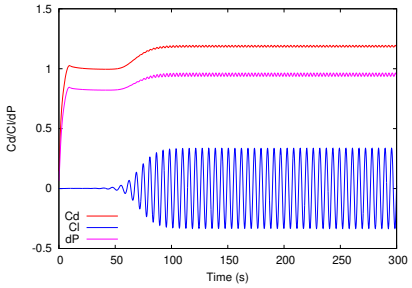

Fig. 2: Time evolution of drag coefficient (C_d), lift coefficient (C_l), and pressure drop across the cylinder's leading and trailing surfaces (dP).

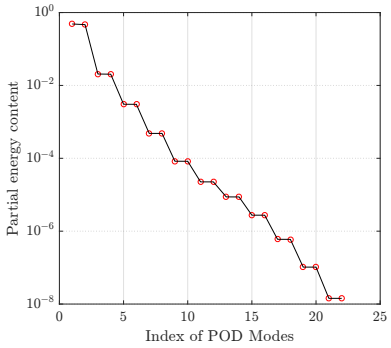

Fig. 3: Eigenvalues spectrum of the POD modes.

pairs of modes, the amplitude keeps reducing subsequently, consistent with the energy spectrum represented in Fig. 3. The frequency of the dynamics of the first pair of modes is half of that of the second pair. The spatial mode pairs are shifted spatially as a result of the convective nature of the flow. The first spatial mode pair ($\boldsymbol{\phi}_1^{\mathrm{POD}}$ and $\boldsymbol{\phi}_2^{\mathrm{POD}}$) jointly depicts the dynamical vortex shedding and their downstream convection. The next mode pairs (($\boldsymbol{\phi}_i^{\mathrm{POD}}$, $\boldsymbol{\phi}_{i+1}^{\mathrm{POD}}$) for $i = 3, 5, \ldots, N_{\mathrm{Gal}}$) correspond to smaller scale structures attributed to the manifestation of the separated shear layers along the sides of the cylinder and their longitudinal expansion further downstream. It must be noted that the length and time scales have been non-dimensionalised by the diameter of the cylinder $D = 1$ m and the cycle time of the vortex shedding $T_c = 0.33$ s, respectively, leading to $x^* = x/D$, $y^* = y/D$ and $t^* = t/T_c$.

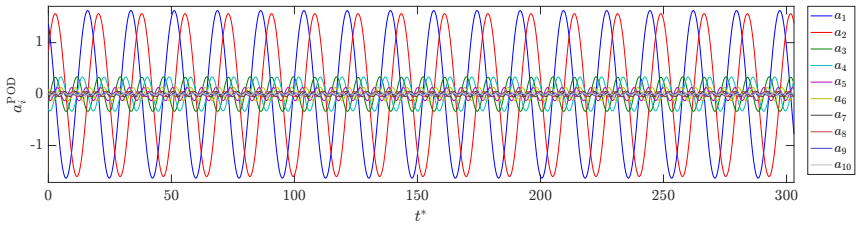

Fig. 4: Time evolution of the temporal POD coefficients a_i^{POD} for $i = 1, \ldots, 10$ corresponding to the most energetic modes for the $2D$-cylinder wake flow at $Re = 100$.

Finally, knowing the time evolution of the temporal POD modes, we can apply the identification method described in § 2.2. For the DA application, the initial parameters of the ROM are identified using the first 450 snapshots cor-

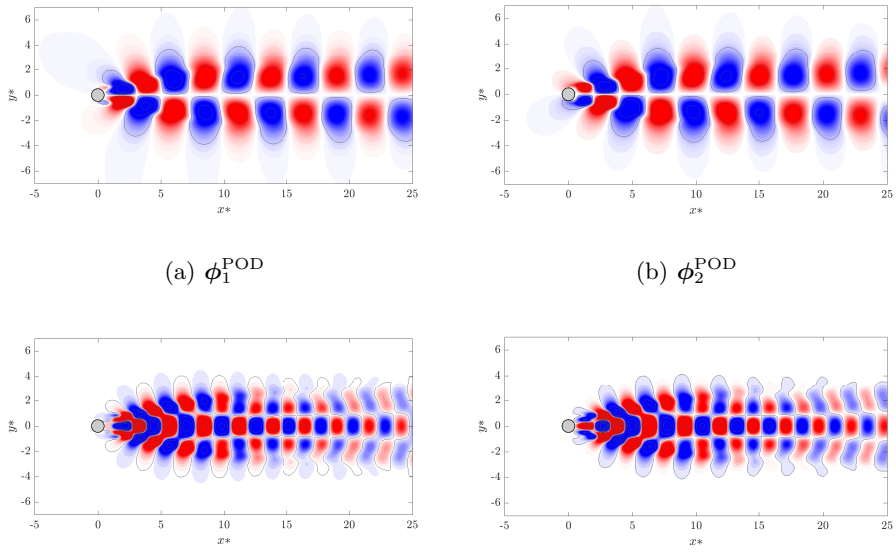

(a) $\boldsymbol{\phi}_1^{\mathrm{POD}}$ (b) $\boldsymbol{\phi}_2^{\mathrm{POD}}$

(c) $\boldsymbol{\phi}_3^{\mathrm{POD}}$ (d) $\boldsymbol{\phi}_4^{\mathrm{POD}}$

Fig. 5: Spatial POD modes $\boldsymbol{\phi}_i^{\mathrm{POD}}$ corresponding to the four most energetic modes for the $2D$-cylinder wake flow at $Re = 100$.

responding to $t^* \in [0, 136.4]$, the next 450 snapshots corresponding to $t^* \in (136.4, 272.8]$ being used for verification of the procedure.

As already discussed, the POD ROM is in general not sufficiently accurate to describe the original dynamics followed by the POD modes. This is illustrated in Fig. 6 where the ROM built using the parameter values obtained from the least-mean-square minimisation (see § 2.2) and without the model eddy viscosity, *i.e.* $\nu_i^T = 0$ (for all $i = 1, \ldots, N_{\mathrm{Gal}}$) is employed to determine the time evolution of the POD coefficients hereafter denoted as $a_i^{\mathrm{ROM}-0}$. We observe that after certain time within the integration window, the true dynamics are not exactly captured by the identified ROM. This is the main motivation to use a DA method like the Dual EnKF to correct the values of the ROM parameters.

4 Results of Dual EnKF assimilation

The estimation of the state and model parameters is performed by tracking the dynamical system. The configuration of the observer and the estimation results are discussed in this section.

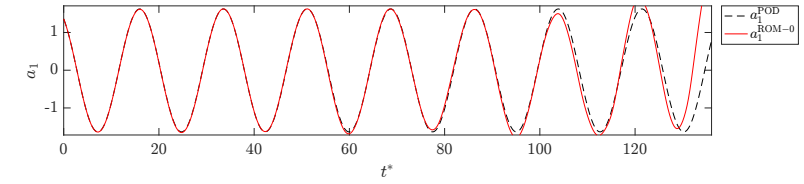

(a) a_1

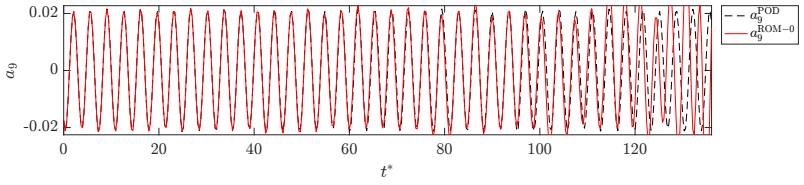

(b) a_9

Fig. 6: True a_i^{POD} (dashed) and estimated $a_i^{\mathrm{ROM-0}}$ (solid) temporal POD modes ($i = 1, 9$) obtained with the identified POD ROM ($N_{\mathrm{Gal}} = 10$) for the $2D$-cylinder wake flow at $Re = 100$. The parameters of the POD ROM are obtained with a least-mean-square minimization procedure.

4.1 Setup of observations

The observation vector $\boldsymbol{y}$ in (15) is obtained in the form of measurements of the streamwise velocity component u_x at specific locations (probes) in the flow-field. The *representers* introduced in § 3.1 are shown in Fig. 7 for different probe configurations. Here, N_o is equal to the number of probes. By comparing the influence fields of single probe ($N_o = 1$) in Fig. 7a and Fig. 7b, it can be concluded that the measurements taken at points with relatively lower variations have lower contribution to the state correction. In this paper, the DA is performed with multiple probes ($N_o = 14$) which gives a higher magnitude of influence than the single probes as shown in Fig. 7c.

The fluctuating component u_x' is obtained after subtracting the temporal mean of the measurements over the assimilation window. The measurements are sampled at the same frequency and instants as the flow snapshots. The spatial POD eigenfunction corresponding to each probe serves as the linear observation operator which maps the temporal POD modes obtained from the dynamical model to the observed fluctuation. The observation equation is reformulated as

$$u_x'(\boldsymbol{\chi}_i, t_k) = \sum_{j=1}^{N_{\mathrm{Gal}}} \boldsymbol{\phi}_j^{\mathrm{POD}}(\boldsymbol{\chi}_i) a_j(t_k) + \epsilon_k, \tag{27}$$

where $i = 1, \ldots, N_\chi$, $k = 1, \ldots, N_{t,\mathrm{DA}}$, and $u_x' \in \mathbb{R}^{N_o}$.

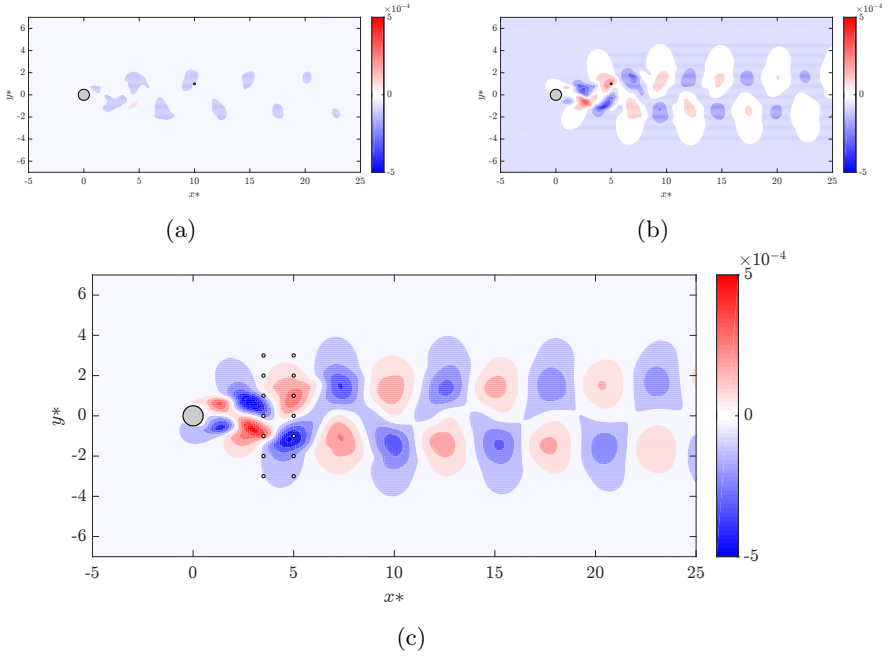

Fig. 7: Measurement influence fields for the streamwise velocity component for different probe configurations (a) $N_o = 1$ located at $(x^*, y^*) = (10, 1)$, (b) $N_o = 1$ located at $(x^*, y^*) = (5, 1)$, and (c) $N_o = 14$ spanning the sub-domain $x^* \in \{3.5, 5\}$, $y^* \in \{-3, 3\}$ with uniform separation of $\Delta x^* = 1.5$, $\Delta y^* = 1.0$. Note that all the figures have the same contour levels.

4.2 State and parameter estimation

In order to separately identify the estimated values of the temporal POD coefficients in the assimilation window, these coefficients are denoted by a_i^{DA} $(i = 1, \ldots, N_{\mathrm{Gal}} = N_s)$. In addition, the size of the parameter space $\boldsymbol{\theta}$ in terms of the model eddy viscosity ν_i^T is $N_p = N_{\mathrm{Gal}}$.

The initial values of the state and parameters and the level of covariances that are used to build the ensemble of the state, parameters and observation are assigned at the start of the assimilation window (see § 2.4). The state and parameters are initialised as $a_i^{\mathrm{POD}}(t^* = 0)$ and $\nu_i^T = 10^{-3}$, respectively, for $i = 1, \ldots, N_{\mathrm{Gal}}$. The covariance matrices are fixed for the whole assimilation window as $\boldsymbol{Q}_k = 10^{-8}\boldsymbol{I}_{N_{\mathrm{Gal}}}$ for the state and $\boldsymbol{R}_k = 10^{-6}\boldsymbol{I}_{N_o}$ for the observations. The parameter covariance matrix is fixed as $\boldsymbol{C}_k = 10^{-4}\boldsymbol{I}_{N_p}$. This choice of covariance levels reflects the relatively higher confidence in the dynamical and observation models as compared to confidence in the dynamical model parameters. The ensemble size of the state and parameter space is $N_e = 50$.

The results of the Dual-EnKF assimilation for the POD-ROM is shown in Fig. 8. Comparing the evolution of the estimated values a_i^{DA} in the assimilation

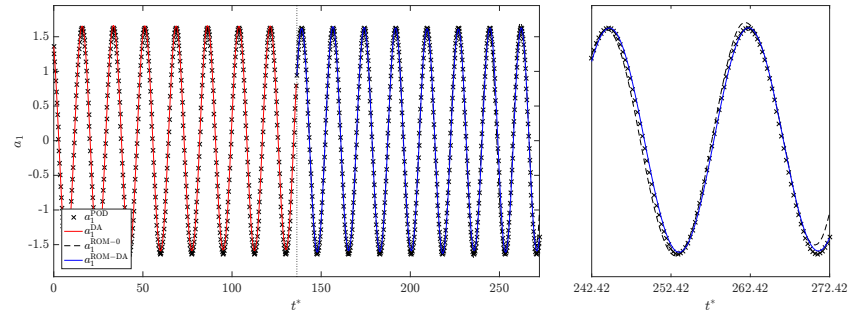

(a) a_1

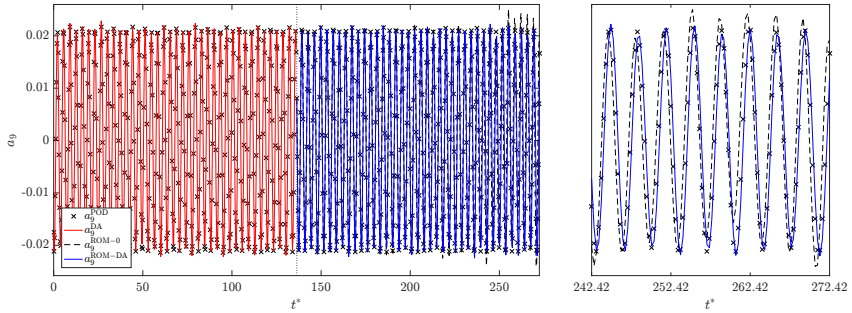

(b) a_9

Fig. 8: Evolution of the temporal coefficients a_i $(i = 1, 9)$. The estimated a_i^{DA} and forecasted $a_i^{\mathrm{ROM-DA}}$ values are compared to the true values a_i^{POD}. The forecasted values are also compared with the results of the POD ROM $a_i^{\mathrm{ROM-0}}$ with no model eddy viscosity ($\nu_i^T = 0$). The dotted line at $t^* = 136.4$ indicates the end of the assimilation window and beginning of the forecast window. The plots on the right hand side (top and bottom) show the magnified view at the end of the forecast window.

window ($t^* \leq 136.4$) with the results obtained from the POD ROM as shown in Fig. 6, we observe that the ensemble Kalman filter enables the model to faithfully recover the trajectory corresponding to the POD modes a_i^{POD}. This reproduction of the true background trajectory is also important with respect to the parameter update. Indeed, by definition of the Dual EnKF method, the model parameters (model eddy viscosity), are also updated simultaneously under the influence of the state estimation. This parameter evolution within the assimilation window is shown in Fig. 9. All the parameters evolve to stable values by $t^* = 100$.

In order to test the long-term stability of the time integration, the POD ROM with the updated model eddy viscosity obtained at the end of the assimilation

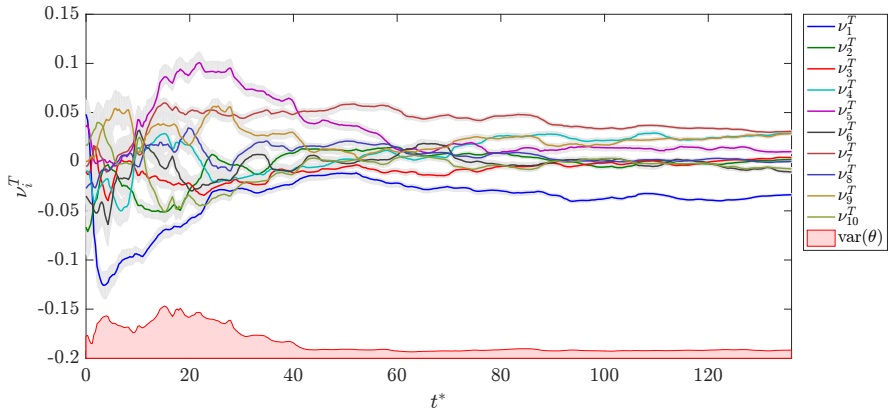

Fig. 9: Evolution of the model eddy viscosity ν_i^T $(i = 1, \ldots, 10)$ of the POD ROM in the assimilation window. The spread of the parameter ensemble throughout the assimilation stage is shown by the grey shaded area. The red shaded area in the bottom shows evolution of the variance of the parameter space $\boldsymbol{\theta} = \{\nu_i^T\}_{i=1}^{10}$ (not to scale).

window is used to forecast the dynamics. The temporal modes obtained from this updated model are denoted as $a_i^{\mathrm{ROM-DA}}$ to highlight the corrections introduced by DA. The initial value for the forecast is taken at the end of the assimilation window as $a_i^{\mathrm{POD}}(t^* = 136.4)$. The result is shown in Fig. 8 for $t^* > 136.45$ in continuation to the assimilation. The evolution is compared with the true values a_i^{POD} and $a_i^{\mathrm{ROM-0}}$ which is the temporal evolution of the POD ROM without the model eddy viscosity, *i.e.* $\nu_i^T = 0$ for $i = 1, \ldots, N_{\mathrm{Gal}}$. It is observed that the true values are faithfully reproduced and the characteristic instability of the POD ROM without the model eddy viscosity terms is no longer present. This effect is more prominent at the end of the forecast window and for the less energetically dominant mode $(i = 9)$. The performance is quantified by calculating the root-mean-square error (RMSE) of the forecasted streamwise velocity obtained from both the models. By definition, we have

$$\mathrm{RMSE}(t) = \sqrt{\frac{1}{N_\chi} \sum_{i=1}^{N_\chi} \left(u_x^{\mathrm{est}}(\boldsymbol{\chi}_i, t) - u_x(\boldsymbol{\chi}_i, t)\right)^2}, \tag{28}$$

where u_x^{est} is the estimated velocity determined either with the coefficients $a_i^{\mathrm{ROM-0}}$ or $a_i^{\mathrm{ROM-DA}}$. The time evolution of RMSE is shown in Fig. 10. The gain in stability of the POD ROM with the assimilated values of the model eddy viscosity is evident from the bounded forecast error. Especially, for $t^* > 260$, the RMSE is lower than the forecast error obtained from the ROM without the model eddy

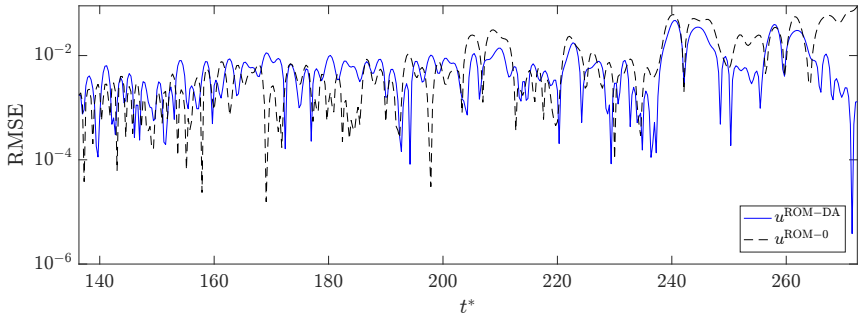

Fig. 10: Time evolution of RMSE of the forecasted variables ${u_x}^{\mathrm{ROM-0}}$ and ${u_x}^{\mathrm{ROM-DA}}$.

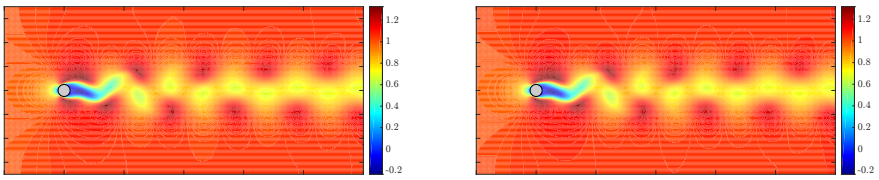

(a) u_x (b) $u_x^{\mathrm{ROM-DA}}$

Fig. 11: True and reconstructed instantaneous streamwise velocity field at the end of forecast, $t^* = 272.8$.

viscosity terms. This result highlights the robust long time performance of the assimilated ROM and also the ability of the assimilation method to provide the correct value of the parameters from sparse observations. Finally, once the temporal POD coefficients have been determined, the already known spatial POD eigenfunctions and mean field can be used in (1) to recover the instantaneous velocity fields as shown in Fig. 11.

5 Conclusion

The Dual EnKF data assimilation is a well-established method in meteorology. It combines different inhomogeneous sources of information (data, dynamical model) for the dual estimation of the true state and model parameters. This allows the prediction of the dynamical evolution with time. In this paper, this approach has been applied in a fluid mechanics context to a POD ROM of a 2D-cylinder wake flow at low Reynolds number ($Re = 100$). We observe that the initial POD ROM obtained from identification is not sufficiently stable to be used for the prediction of the long-term dynamics. Therefore, we apply the

Dual EnKF algorithm to identify the model parameters. During the assimilation, the sparse observations of the streamwise velocity obtained from probes placed in the flow domain are used to simultaneously estimate the state and model parameters. These parameters correspond to the model eddy viscosity introduced in the Galerkin POD ROM to account for the mode truncation. At the end of the assimilation window, with the updated values of the parameters, the ability of the POD ROM to forecast the flow dynamics is characterised.

The Dual-EnKF method provides a robust estimation of the state in the assimilation window by combining the results of the dynamical model (POD ROM) and the measurements. The parameters simultaneously evolve and attain stable values by the end of the assimilation procedure. The POD ROM with the updated parameters provides a stable and more accurate estimate of the long-term dynamics as compared to the ROM without the model eddy viscosity terms.

As an extension of current work, the influence of the initial covariance levels of the state, parameter and observations on the performance of the assimilation method must be studied. Also, the numerical test case studied here features a large fraction of energy captured by a few dominant modes. This limits the scope of improvement of the dynamical model by the application of DA. Therefore, in the future, a similar study will be performed on more chaotic experimental flow cases. Also, the influence field of the probes may be used to propose a methodology for optimal sensor placement.

References

[1] M. Bergmann and L. Cordier. Optimal control of the cylinder wake in the laminar regime by trust-region methods and pod reduced-order models. *Journal of Computational Physics*, 227(16):7813–7840, 2008.

[2] L. Cordier and G. Tissot. Model Reduction, POD and Data Assimilation. In *Lecture series 2014-01 on Advanced Post-Processing of Experimental and Numerical Data*, pages 1–89. Von Kármán Institute for Fluid Dynamics, 2013. ISBN 978-2-87516-061-4.

[3] L. Cordier, B. Abou El Majd, and J. Favier. Calibration of POD Reduced-Order Models using Tikhonov Regularization. *International Journal for Numerical Methods in Fluids*, 2:63, 2010.

[4] G. Evensen and P. J. Van Leeuwen. Assimilation of geosat altimeter data for the agulhas current using the ensemble kalman filter with a quasigeostrophic model. *Monthly Weather Review*, 124(1):85–96, 1996.

[5] F. Hecht. New development in FreeFem++. *Journal of Numerical Mathematics*, 20(3-4):251–265, 2012.

[6] J. L. Lumley. Atmospheric Turbulence and Wave Propagation. the structure of inhomogeneous turbulence. pages 166–178, 1967.

[7] H. Moradkhani, S. Sorooshian, H. V. Gupta, and P. R. Houser. Dual state-parameter estimation of hydrological models using ensemble Kalman filter. *Advances in Water Resources*, 28(2):135 – 147, 2005.

[8] N. Papadakis. *Assimilation de données images : Application au suivi de courbes et de champs de vecteurs*. Phd thesis, Université de Rennes I, 2007.

[9] L. Perret, E. Collin, and J. Delville. Polynomial identification of POD based low-order dynamical system. *Journal of Turbulence*, (7):N17, 2006.

[10] D. Rempfer and H. F. Fasel. Evolution of three–dimensional coherent structures in a flat–plate boundary layer. *Journal of Fluid Mechanics*, 260:351–375, 1994.

[11] C. W. Rowley and S. T. M. Dawson. Model Reduction for Flow Analysis and Control. *Annu. Rev. Fluid Mech.*, 49(1):387–417, 2017.

[12] A. F. C. da Silva. *An EnKF-based flow state estimator for aerodynamic problems*. Phd thesis, California Institute of Technology, 2019.

[13] L. Sirovich. Turbulence and the dynamics of coherent structures. I. Coherent structures. *Quarterly of Applied Mathematics*, 45(3):561–571, 1987.

[14] O. Talagrand and P. Courtier. Variational Assimilation of Meteorological Observations with the Adjoint Vorticity Equation. I: Theory. *Quarterly Journal of the Royal Meteorological Society*, 113(478):1311–1328, 1987.